One-dimensional excitonic states and lasing in highly uniform quantum wires formed by cleaved-edge overgrowth with growth-interrupt annealing

2004 J. Phys.: Condens. Matter 16 S3549

(http://iopscience.iop.org/0953-8984/16/35/001)

INSTITUTE OF PHYSICS PUBLISHING JOURNAL OF PHYSICS: CONDENSED MATTER

J. Phys.: Condens. Matter **16** (2004) S3549–S3566 PII: S0953-8984(04)83324-1

One-dimensional excitonic states and lasing in highly uniform quantum wires formed by cleaved-edge overgrowth with growth-interrupt annealing

H Akiyama[1,2], M Yoshita[1,2], L N Pfeiffer[2] and K W West[2]

[1] Institute for Solid State Physics (ISSP), University of Tokyo, and CREST, JST, 5-1-5 Kashiwanoha, Kashiwa, Chiba 277-8581, Japan
[2] Bell Laboratories, Lucent Technologies, Murray Hill, NJ 07974, USA

Received 6 July 2004
Published 20 August 2004
Online at stacks.iop.org/JPhysCM/16/S3549
doi:10.1088/0953-8984/16/35/001

Abstract

High quality T-shaped quantum wire lasers are fabricated by cleaved-edge overgrowth with molecular beam epitaxy on an interface improved by a growth-interrupt high temperature annealing. Microphotoluminescence and photoluminescence (PL) excitation spectroscopy at low temperatures reveals the formation of quantum wires with unprecedentedly high quality, and intrinsic structures of one-dimensional (1D) free excitons, exciton excited states, and 1D continuum states. At high pumping levels, the PL evolves from showing a sharp free exciton peak via exhibiting a biexciton peak to a Coulomb correlated electron–hole plasma PL band. Lasing has been achieved with a low lasing threshold, and its emission patterns are measured in imaging experiments. The lasing energy is in the plasma PL band and is about 5 meV below the free exciton level. The observed shift excludes the possibility of free excitons in the lasing, and suggests a contribution from the electron–hole plasma. Single T-wire samples such as a single-quantum-wire laser and a field-effect-transistor-type doped single quantum wire are fabricated and studied optically.

(Some figures in this article are in colour only in the electronic version)

1. Introduction

A quantum wire laser was first achieved by Kapon and co-workers [1] in 1989, although the lasing occurred only at higher subbands in multimode wires. In 1993, Wegscheider and co-workers [2] demonstrated ground state lasing in quantum wires. They found that the lasing energy was exactly at the peak of the excitonic spontaneous emission, and was nearly independent of the pump levels. This suggested the absence of band-gap renormalization and an enhanced stability of one-dimensional (1D) excitons. Therefore, the gain was ascribed to

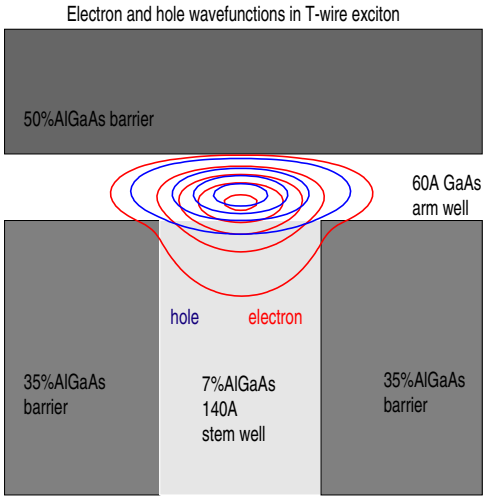

Figure 1. The exciton in a T-shaped quantum wire structure calculated by Szymanska *et al* [12].

excitons, and this claim has stimulated wide interest in the fields of basic and applied physics for about ten years [3–9].

In general, it is believed that lower dimensional semiconductor lasers show better performance due to a more concentrated density of states at the lowest energy [10, 11]. In fact, 2D quantum well lasers have superior characteristics to 3D double heterolasers. As for 1D quantum wire lasers and 0D quantum dot lasers, however, fabrication of uniform structures having sharp density-of-states features is very difficult, and the superior performances have not been confirmed yet.

In this paper, we present the fabrication of high quality T-shaped quantum wire lasers by the cleaved-edge overgrowth method and growth-interrupt annealing technique with molecular beam epitaxy (MBE), and review our recent results from photoluminescence (PL), PL excitation (PLE), and optically pumped lasing measurements.

2. T-shaped quantum wires and lasers

Figure 1 shows the schematic structure [12] of a T-shaped quantum wire (T-wire) used in the present work. A quantum wire state is formed quantum mechanically at a T-intersection of two quantum wells, denoted as a stem well and an arm well. Here, the stem well is a 14 nm 7% AlGaAs well with 35% AlGaAs barriers, whereas the arm well is a 6 nm GaAs well with a 50% upper barrier. The contour curves in the figure show wavefunctions of an electron and a hole in a ground state exciton.

Figure 2 shows the structure of a quantum wire laser sample consisting of 20 wires of 14 nm by 6 nm size separated by 42 nm 35% AlGaAs barriers, which are embedded in an optical waveguide of T-shaped core layers and 50% AlGaAs cladding layers. The wafer was cleaved into laser bars with a typical cavity length of 500 μm with uncoated facet mirrors.

3. Growth-interrupt annealing with cleaved-edge overgrowth

The T-wire structures are fabricated by the cleaved-edge overgrowth method [13] by MBE, in which two-step growth processes are separated by an *in situ* wafer cleavage process. However,

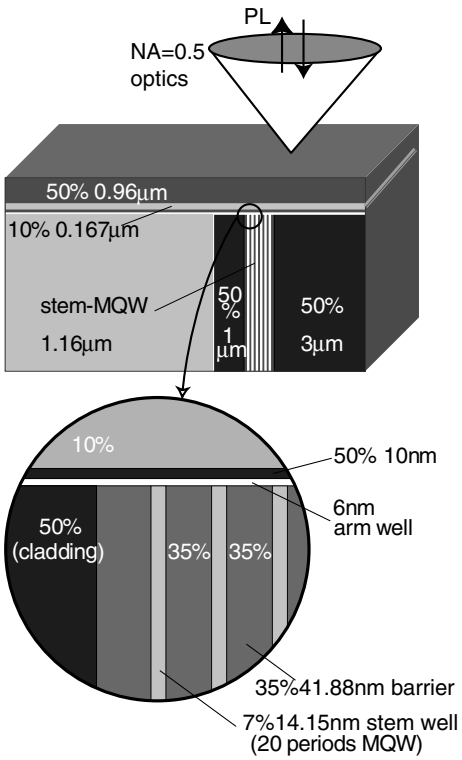

Figure 2. A schematic structure of a T-shaped quantum wire laser sample with 20 wires of 14 nm by 6 nm size.

a difficulty lies in the second MBE growth of an arm well on a (110) cleaved surface, which requires a low substrate temperature of 490 °C under a high As_4 overpressure. In fact, the as-grown surface of an arm well shows large roughness, as shown in the AFM image of figure 3(a).

To solve [14] this problem, we developed an *in situ* annealing technique, in which growth is interrupted at elevated temperatures for surface annealing. As shown in the AFM images in figures 3(b)–(d), this technique dramatically improves the surface morphology of the arm well surface. In particular, annealing at 600 °C for 10 min results in an atomically flat surface without roughness over a 100 μm region (lateral extent).

To further investigate [15] the driving force of the formation of the atomically flat surface, we introduced an additional amount of GaAs by adding fractional MLs to the 30 ML GaAs film, and studied the surfaces after annealing at 600 °C for 10 min. As shown in the AFM images in figure 4, we found characteristic patterns formed on (110) surfaces, *boat*-shaped 2–3 ML high islands and *tropical-fish*-shaped 1 ML deep pits, which suggest an adatom migration model on the (110) GaAs surface [15, 16].

Note the large lateral sizes of the *fish*-shaped pits and island–island distance which indicates a long adatom migration length on the (110) GaAs surface at 600 °C. We confirmed this effect by first-principles calculations [17], where potential barrier energies of atom migration on a (110) GaAs surface were calculated on the basis of density functional theory within the generalized gradient approximation. The result shown in figure 5 revealed that the Ga atom migration is one-dimensional and the migration barrier energy is smaller than that on a (001) GaAs surface.

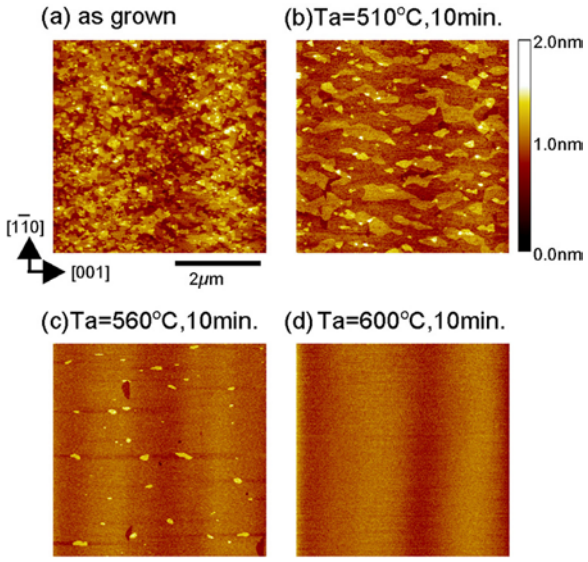

Figure 3. AFM images of the top surface of a 5 nm thick arm well grown at 490 °C on a (110) cleaved edge by the cleaved-edge overgrowth method, and then *in situ* annealed at elevated temperatures for 10 min [14].

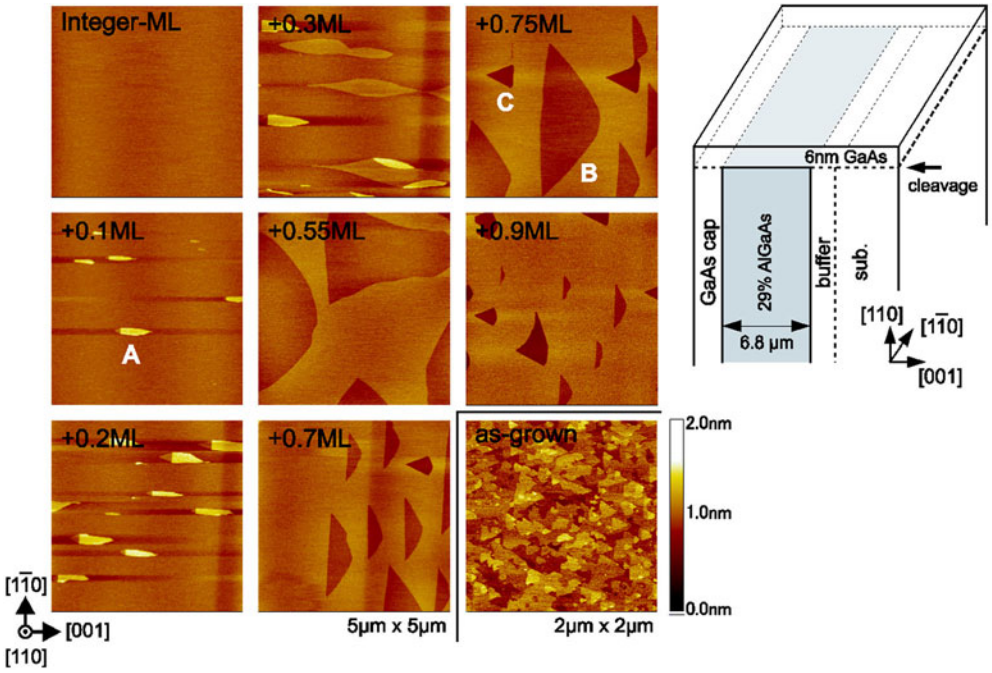

Figure 4. AFM images of the surface of a 6 nm thick (110) GaAs layer grown on a cleaved (110) edge of a 6.8 μm thick 29% AlGaAs layer on the (001) substrate. A schematic sample structure is shown in the inset. The (110) GaAs layer was overgrown at 490 °C under As_4 flux. After the overgrowth, *in situ* annealing of the surface was carried out at 600 °C for 10 min. A position with integral ML deposition is denoted as 'Integer-ML', and other positions with fractional ML are denoted by the deviations of the deposition from the integral ML. As a reference, the AFM image of the surface without annealing appears, labelled 'as-grown' [15].

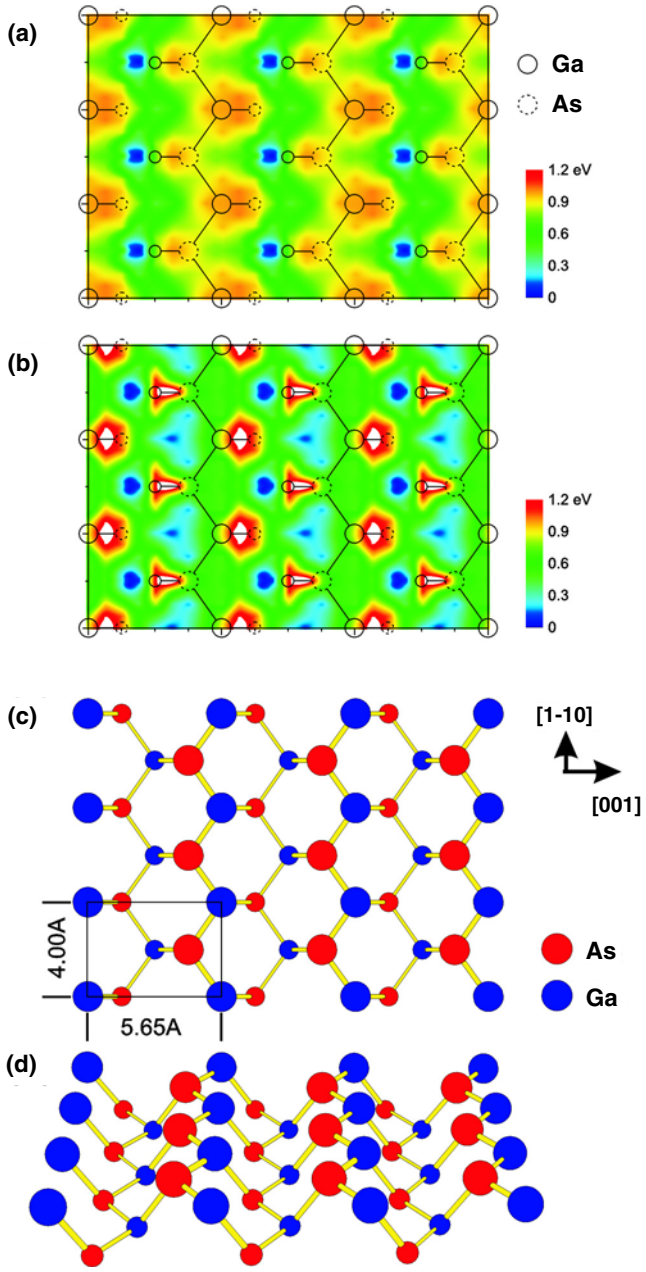

Figure 5. A contour map of the migration barrier energy for (a) a Ga adatom and (b) an As adatom on a GaAs(110) surface with the surface atomic configuration. The dotted and solid circles correspond to As and Ga, respectively. ((c), (d)) Atomic models of a GaAs(110) surface. Larger and smaller circles correspond to the first and second atomic layers from the surface [17].

Covering the GaAs surfaces shown in figure 4 with AlGaAs barriers, we fabricated quantum well structures. Micro-PL spectroscopic study [15] has shown that the atomically flat interfaces are conserved. Investigations of interesting problems such as the PL width and

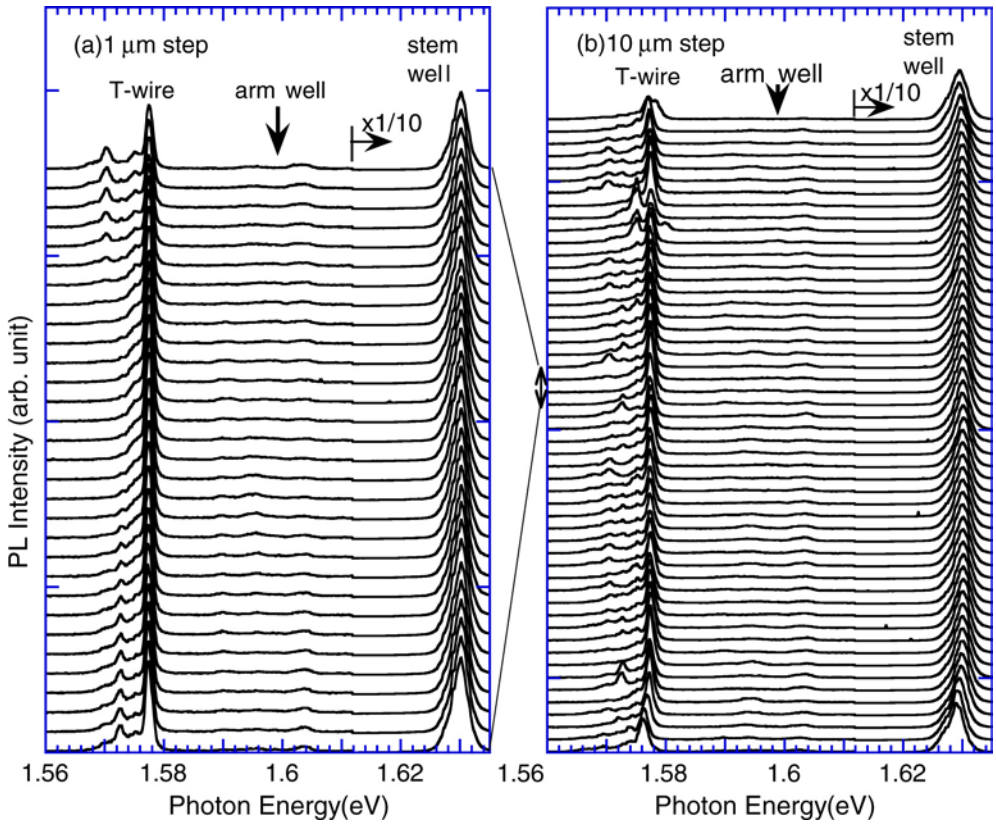

Figure 6. Micro-PL spectra at 5 K scanned along the quantum wires (a) in 1 μm steps for 30 μm and (b) in 10 μm steps for 500 μm [18].

electron–hole carrier migration in quantum wells with atomically flat interfaces are now in progress.

4. The 1D exciton ground state, excited states, and continuum states

Figure 6 shows micro-PL spectra [18] scanned along the wires at 5 K, measured in the configuration shown in figure 2, (a) in 1 μm steps for a 30 μm region and (b) in 10 μm steps for the whole cavity length of 500 μm. The high energy peaks show the PL of the stem wells, and the low energy peaks show the PL of T-wires. PL of the arm well is not observed because carriers generated in the arm well quickly flow into adjacent low energy wire states. The PL of T-wires has a main exciton peak and lower energy small peaks. The small PL peaks show intensity fluctuations at descrete energy positions, and are ascribed to localized excitons due to monolayer islands in the arm well. The strong and uniform intensity of the main peak and small intensity of the localized exciton peak show the high uniformity of the sample.

Figure 7 shows (a) PL and (b) PLE spectra [18] of the quantum wires at a central position of figure 6(a). The sharp PL width of 1.5 meV was observed for the T-wires, as shown in figure 7(a), which is about an order of magnitude narrower than that for previous wires formed without annealing. In the PLE spectrum of figure 7(b), we found exciton absorption peaks of the T-wires, the arm well, and the stem wells. The Stokes shift of the T-wire exciton peak is

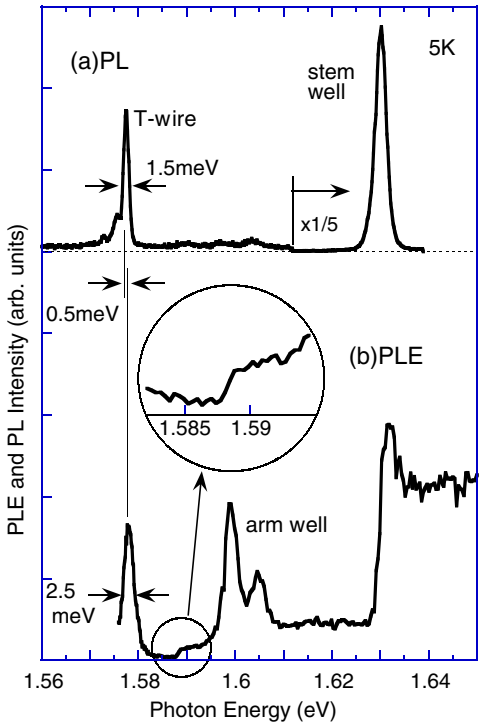

Figure 7. (a) PL and (b) PLE spectra of T-wires at 5 K [18].

0.5 meV, much smaller than the PL and PLE widths, which suggests that the wire PL is mostly coming from free excitons.

Note that a small continuous absorption band is observed with an onset at 11 meV above the ground state exciton peak of the T-wires. This is ascribed to 1D ionized continuum states. Note that the $1/\sqrt{E}$ singularity due to the 1D density of states is absent at the onset of the continuum absorption band. This effect was predicted theoretically more than ten years ago [19].

To investigate finer spectral features, we performed numerical calculations [20] for 1D exciton states, where we assume a T-wire geometry in a 3D box with a finite size, but calculate complete sets of electron and hole wavefunctions and perform exact diagonalization of the Coulomb interaction matrix elements [12]. Figure 8 shows the wavefunctions of the excitonic states obtained. The wavefunctions show, for example, that the first state is the ground exciton state, and that the second state is the first exciton state formed between the first electron subband and the second hole subband. Figure 9 shows the calculated absorption energies and intensities of these exciton states (open circles), in comparison with the measured polarization-dependent PLE spectra (solid and dashed curves) [20]. The energies of the first, second, and continuum states show good agreement between the experiment and the theory.

5. Formation of biexcitons and an electron–hole plasma with strong Coulomb correlations

Figure 10(a) shows PL spectra of T-wires at various pumping levels [21]. At low pumping levels, free excitons dominate the PL spectra. As the pumping level is increased, a new emission band grows at 3.2 meV below the free exciton peak. With increasing pump power

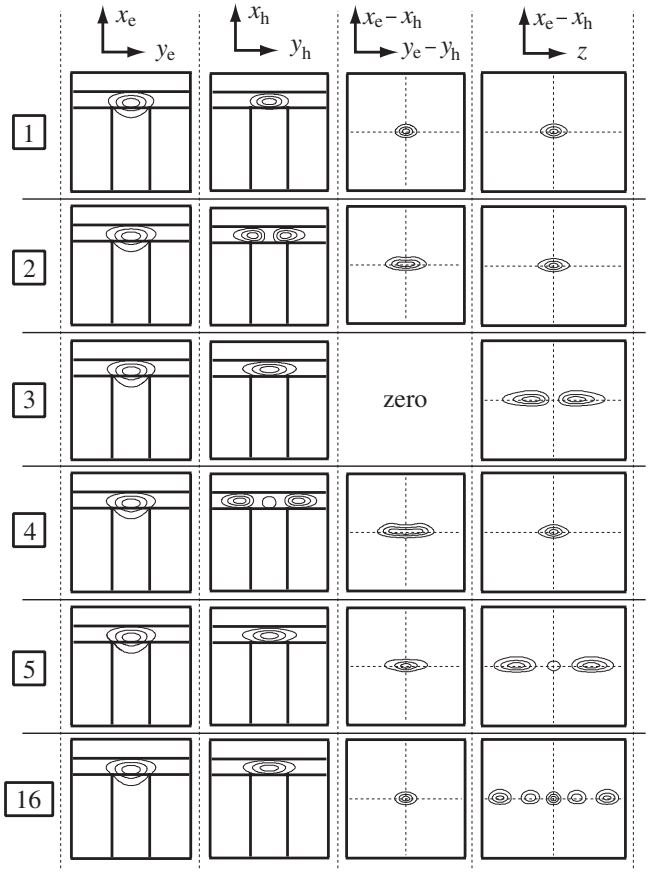

Figure 8. Contour plots of calculated squared wavefunctions ($n = 1, 2, 3, 4, 5$, and 16) for various parameter pairs. Parameters (x_e, y_e, z_e) and (x_h, y_h, z_h) denote the positions of an electron and a hole, and z is defined by $|z_e - z_h|$. The directions of x, y, and z correspond to [110], [001], and $[1\bar{1}0]$. The three contour lines in each box represent 80%, 50%, and 20% of the maximum [20].

this new emission band becomes broader but undergoes no further red-shift. At the higher pump levels the low energy emission band dominates the spectrum and the free exciton peak is quenched.

Figure 10(b) shows log plots of the low energy broad PL band intensities I_2 as a function of the free exciton PL intensities I_1. We find that $I_2 \propto I_1$ at the lowest pump powers due to the contribution of localized excitons in I_2. For higher excitation levels we find that $I_2 \propto I_1^2$. With increasing pump levels we first find larger exponents followed by saturation. In the region of $I_2 \propto I_1^2$, biexcitons are expected to contribute to the red-shifted PL band. For intense photoexcitation the free exciton peak is quenched and is not fully differentiated from the broadened lower energy PL band.

In this high excitation regime, the intense optical emission should be ascribed to a 1D electron–hole plasma confined to the quantum wires. Here densities should be high enough that there are no long lived excitons or exciton complexes. Nevertheless, the low energetic position of the emission, and the absence of further red-shift with photoexcitation at high pump levels, shown in figure 10(a), suggests that the *instantaneous* electron–hole correlations are strong. The state is unlike a free electron–hole plasma, and is better described as a neutral

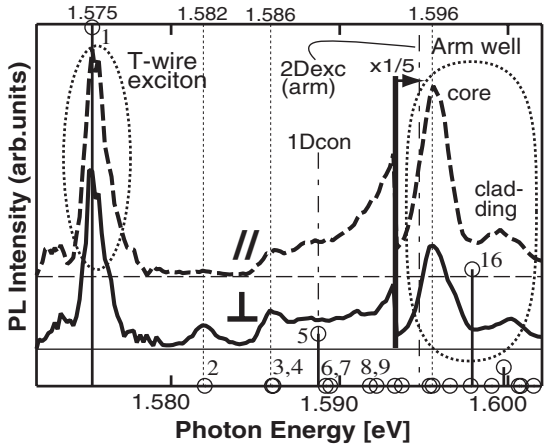

Figure 9. Polarization-dependent PLE spectra of T wires at 5 K with the calculated oscillator strength. The broken curve is for parallel polarization, while the solid curve is for perpendicular polarization. Letters near circles represent the numbers of states. Dotted–dashed curves are for the onset of the 1D continuum state and the peak of the 2D ground state exciton [20].

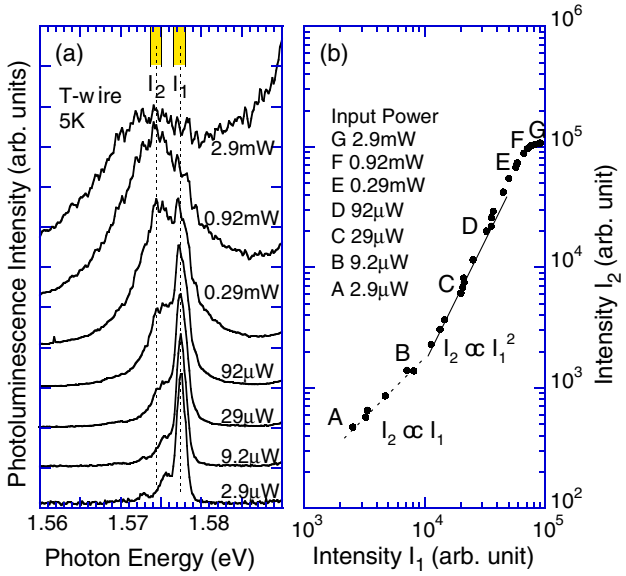

Figure 10. (a) PL spectra of T-wires at various pumping levels and (b) log plots of low energy broad PL band intensities I_2 as a function of the free exciton PL intensities I_1 [21].

electron–hole plasma in which Coulomb correlations fix the peak emission energy to a value that is close to that of the biexciton energy [21].

6. Lasing performances

For stimulated emission measurements [21, 22], two cylindrical lenses and a 0.4 numerical aperture objective lens were used to focus the incident beam into a filament shape with about

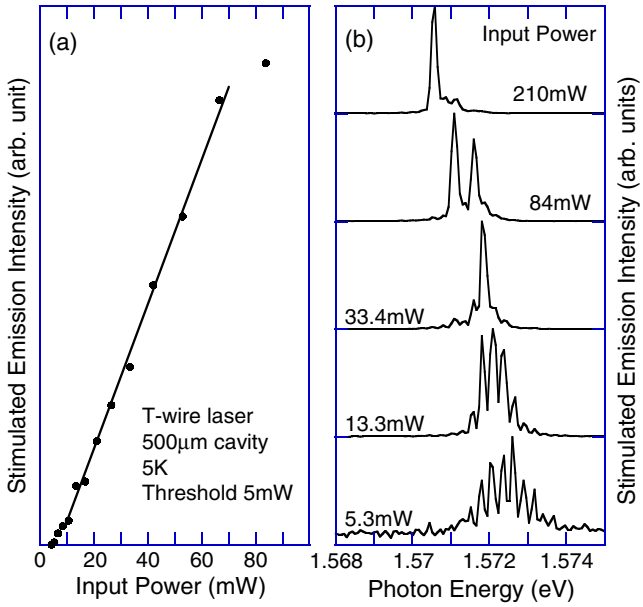

Figure 11. (a) Intensity plots and (b) spectra of stimulated emission from the ground state in the T-wire laser for various input powers [21].

1 μm width to pump the whole 500 μm long laser cavity through the arm well surface (the top surface in figure 2), and the cw output of the excitation laser was mechanically chopped into 0.25 ms rectangular pulses of 1% duty ratio to minimize sample heating. The peak input power per pulse was varied from 0 to 210 mW.

The stimulated emission was collected in the direction of the waveguide through one of the cavity mirror surfaces (the front and rear surfaces in figure 2) and spontaneous emission was simultaneously measured in the direction perpendicular to the waveguide through the top surface of the arm well.

Figure 11 shows (a) the total intensity and (b) spectra of stimulated emission from the T-wire laser for various input powers [21]. Plot (a) shows that the lasing threshold is low, 5 mW, at 5 K. Although the spectral linewidth is limited by our spectrometer, spectrum (b) shows that the lasing just above threshold is multimode. It becomes single mode at an input power of about 30 mW, and then shows mode hopping toward lower energy. Note, however, that the amount of shift is only 2 meV for input power variation of 5 to 210 mW.

Figure 12 shows (a) spectra over a wide energy range and (b) intensity plots of three stimulated emission lines (L1, L2, and L3) from the T-wire laser for various input powers. The bottom arrows indicate the energies of free exciton absorption in the T-wire, arm well, and stem well. Note that wire lasing L1 starts at 5 meV below the free exciton absorption energy of the wires.

Figure 13 shows the results of a microscopic imaging experiment on emission patterns [22]. The white lines in each panel show boundaries of 50% AlGaAs cladding layers (cf figure 2). The black curves in panel (a) show the calculated optical mode of the T-shaped optical waveguide and the false-colour image shows its convolution with a Gauss resolution function of 0.8 μm width. The panels (b), (c), and (d) show PL emission patterns below the lasing threshold of the T-wires, arm well, and stem wells, respectively, and confirm the assignment. In particular, image (b) agrees well with (a). Panels (e), (f), and (g) show laser emission patterns of L1, L2

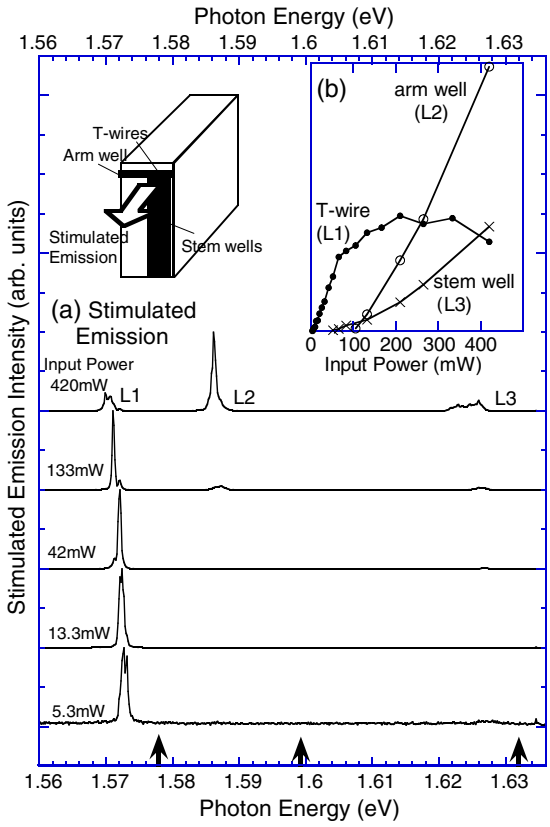

Figure 12. (a) Spectra over a wide energy range and (b) intensity plots of stimulated emission (L1, L2, and L3) from the T-wire laser for various input powers. The bottom arrows indicate the energies of free exciton absorption in the T-wire, arm well, and stem well.

and L3. This supports the conclusion that the origins of L1 and L3 are T-wires and stem wells, while the origins of L2 are excited states of T-wires or the arm well in the core region. It is interesting that the patterns of L1 and L2 are circular and small compared with the calculated mode pattern shown in (a).

7. Lasing mechanism

To understand this 5 meV shift [21, 22] of the wire lasing from the wire free exciton energy, we show, in figure 14, simultaneously measured stimulated and spontaneous emission spectra of the T-wire laser at 5 K for input powers of (a) 5.3 mW, (b) 13.3 mW, and (c) 42 mW. In these measurements we employed the geometry shown in the inset to figure 14(a). The dashed traces show the spontaneous emission spectrum for very weak excitation of 0.42 mW. These spectra identify the location of the free exciton emission peak. The spontaneous emission spectra at high excitation levels in figures 14(a)–(c) are very similar to the PL results of figure 10 measured with point excitation.

The results shown in figure 14 reveal that T-wire lasing is observed about 5 meV below the free exciton energy. Since there is no overlap between the lasing energy and the free exciton peak, the gain for lasing cannot be due to free exciton recombination. Instead, the lasing

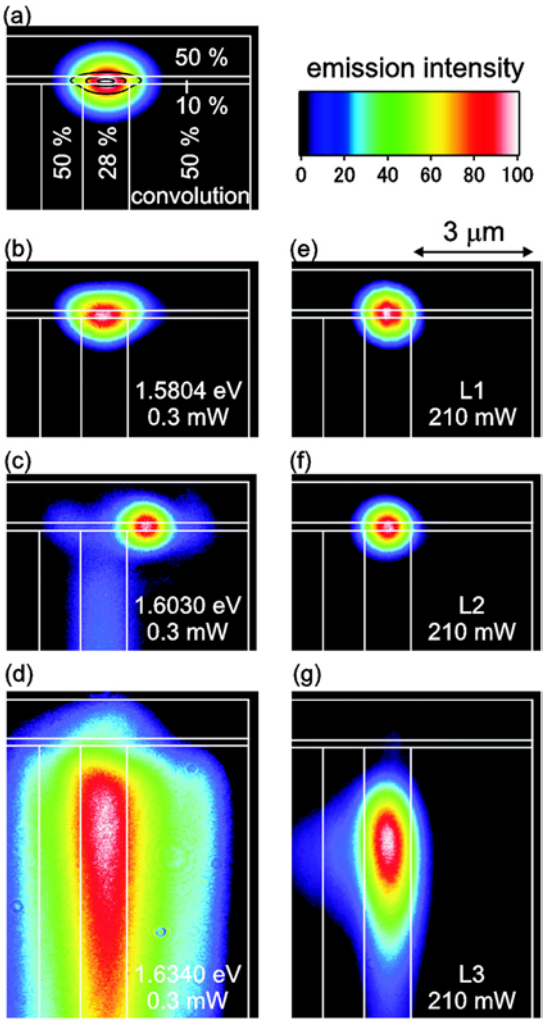

Figure 13. Images of emission patterns in a T-wire laser. White lines superposed on each image represent boundaries of 50% AlGaAs cladding layers. (a) Calculation of the optical mode at the T-shaped waveguide by a finite element method. Black contour curves show the fundamental optical mode and the overlayed image is a convolution with the 0.8 μm spatial resolution function. ((b)–(g)) Microscopic images of emission patterns from a cavity mirror surface measured with spatial resolution of 0.8 μm. Images (b)–(d) are at 0.3 mW and images (e)–(g) are at 210 mW [22].

photon energy overlaps the red-shifted broad PL band. Therefore, we conclude that the gain for lasing is ascribable to the electron–hole plasma with strong Coulomb interactions [21]. The lasing energy is on the low energy side of the plasma emission band, presumably because some absorption may reduce the gain near the peak of spontaneous emission.

8. Single-wire laser

We then fabricated a single-quantum-wire laser, in the 1D quantum limit, which contains only one quantum wire with only one 1D quantized electronic state [23]. Figure 15 shows a

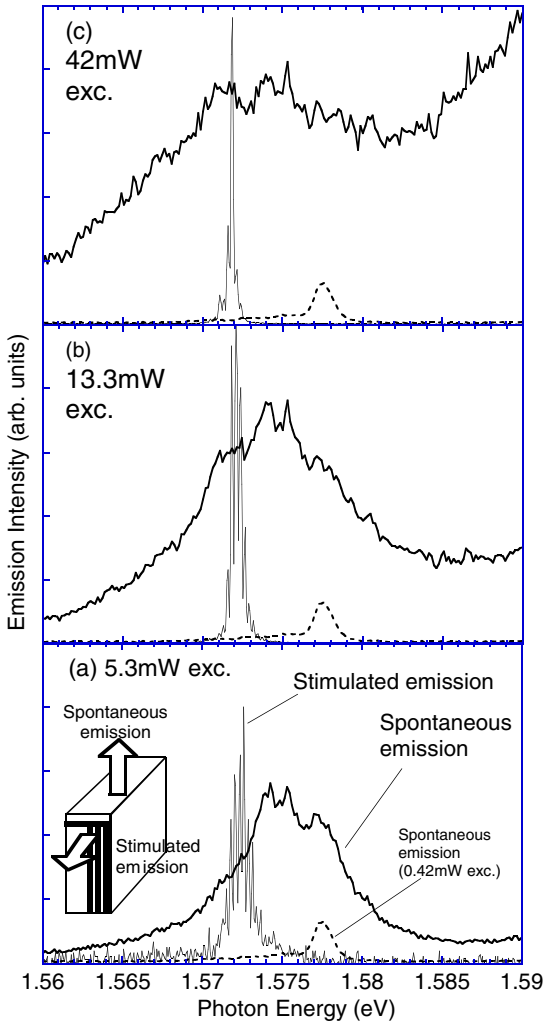

Figure 14. Simultaneously measured stimulated and spontaneous emission spectra of the T-wire laser at 5 K for input powers of (a) 5.3 mW, (b) 13.3 mW, and (c) 42 mW [21].

schematic cross-sectional view of the single-wire laser structure optimized by finite element method calculation. The single T-wire is embedded in the core of a T-shaped optical waveguide formed by two 250 nm 35% AlGaAs layers and a 111 nm 10% AlGaAs layer. A laser bar with a 500 μm optical cavity was cut from the wafer by cleavage, and the cavity mirror surfaces were coated by 120 nm and 300 nm thick gold with estimated reflectivity of about 97%.

The lasing performance of the single-wire laser was measured by means of optical pumping. Figure 16 shows lasing spectra at 5 K measured with the spectral resolution of 0.2 meV. Lasing lines due to the T-wire, arm well, and stem well are observed. The T-wire has fewer longitudinal modes than the arm and stem wells. The inset shows magnified spectra of the T-wire, where several longitudinal modes are denoted. While the input power is low, the T-wire shows multimode lasing with several longitudinal modes. As the input power is increased, the lasing modes become fewer and red-shifted. Note that the red-shift of the stimulated emission peak was as small as 2 meV in spite of the wide variation of the input

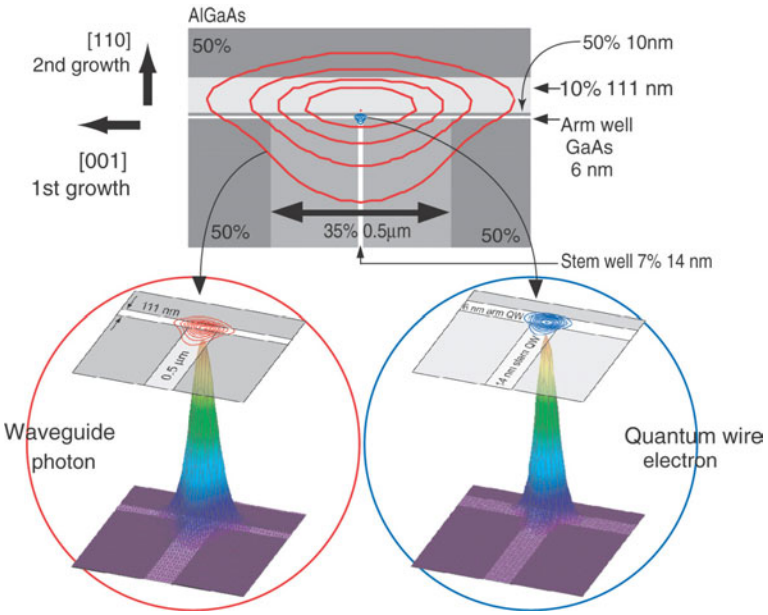

Figure 15. A schematic cross-sectional view of a single-wire laser structure. Percentages show the Al concentration of AlGaAs. A quantum wire (T-wire) is formed at a T-intersection of a 14 nm stem well and a 6 nm arm well, which is embedded in the core of a T-shaped optical waveguide formed from a 500 nm 35% AlGaAs stem layer and a 111 nm 10% AlGaAs arm layer. The squared wavefunctions, or probabilities, for photons and electrons in the device are drawn as contour curves and 3D graphs; these show that photons and electrons are confined at the T-intersections. The optical confinement factor Γ of the T-wire is 5×10^{-4} [23].

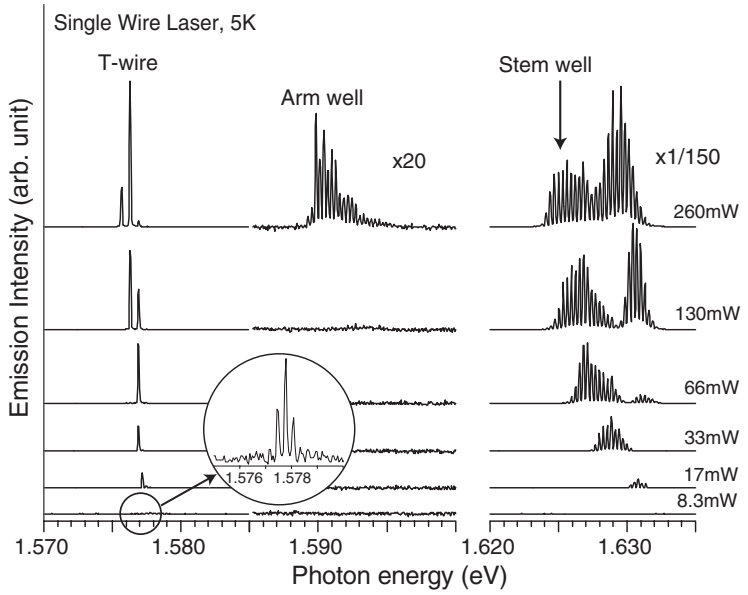

Figure 16. Lasing spectra of the single-quantum-wire laser at 5 K for the various input powers of $P_{in} = 8.3$, 17, 33, 66, 130, and 260 mW, measured with spectral resolution of 0.2 meV. Lasing lines due to the T-wire, the arm well, and the stem well are observed. The lasing of the T-wire has excellent characteristics of a low threshold, a single lasing mode, and small red-shifts [23].

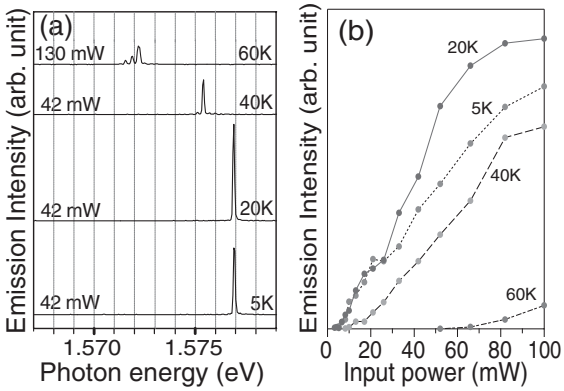

Figure 17. (a) Lasing spectra of the single T-wire at 5, 20, 40, and 60 K. Input powers for respective spectra are indicated in the figure. Stable single-mode lasing is observed up to 40 K. The spectral red-shift of the lasing energy with increasing temperature is due to the shrinkage of the band-gap energy. (b) Laser emission intensity plots for the single T-wire at 5, 20, 40, and 60 K against input powers up to 100 mW [23].

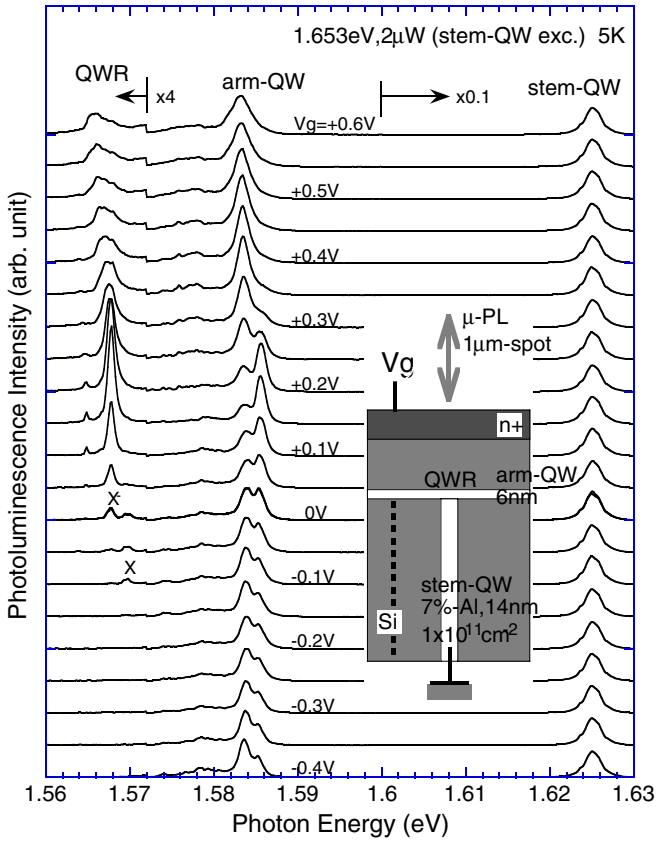

Figure 18. PL spectra at 5 K for various gate voltages V_g, in 0.05 V steps. The inset shows the schematic structure of the T-wire, stem well, arm well, and a gate. Electrons are accumulated or depleted in the T-wire by means of positive or negative V_g [24].

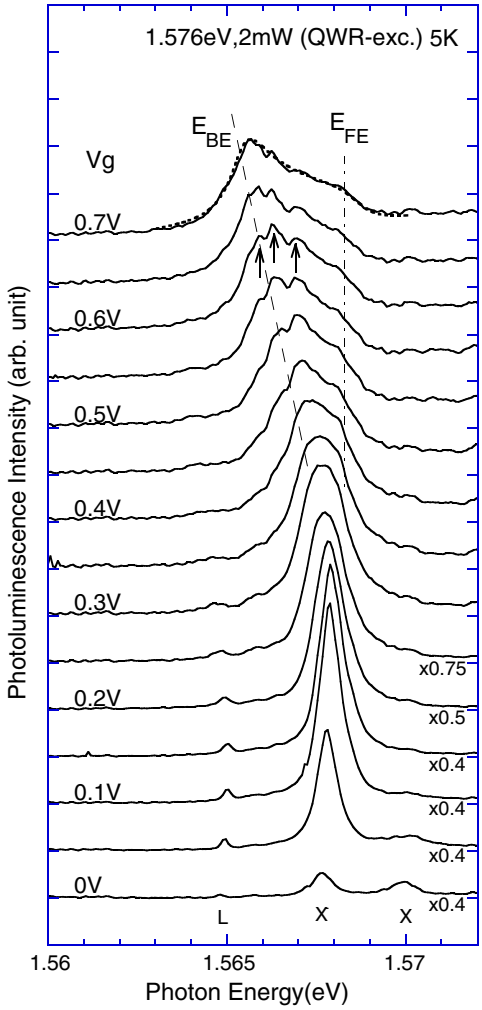

Figure 19. PL spectra of the T-wire at 5 K for positive gate voltages V_g measured in 0.05 V steps. The dashed line and a vertical dash–dot line are drawn to guide the eyes, and indicate the red-shifted band edge E_{BE} and Fermi edge E_{FE} singularity [24].

power. The lasing mode separation is 0.34 meV below the input power of 130 mW, while it becomes 0.68 meV above it.

Lasing due to the T-wire was observed for 5–60 K. Figure 17 plots the laser emission intensity of the T-wire for 5–60 K against the input power up to 100 mW.

9. Doped single wire

To study many-body electron interaction effects in T-wires, we performed PL spectroscopy on a modulation-doped single quantum wire with a gate to tune the 1D electron density [24].

As shown in the inset of figure 18, a single quantum wire is formed at the T-shaped intersection of the 14 nm stem well and the 6 nm arm well, where we introduced a $4 \times 10^{11}\,\mathrm{cm}^{-2}$ Si delta-doping layer with a set-back of 100 nm from the stem well, and a 100 nm thick heavily

Si-doped n^+ 10% AlGaAs gate layer on the arm well with a set-back of 200 nm. We applied a gate voltage to the n^+ gate layer by setting the ground as the n-type modulation-doped stem well (electron density of 1×10^{11} cm^{-2}). Applying a positive or negative DC gate voltage V_g to the n^+ gate layer, we accumulated or depleted additional electrons in the T-wire.

Figure 18 shows PL spectra at 5 K for various gate voltages V_g in 0.05 V steps between -0.4 and 0.6 V. Figure 19 shows PL spectra of the T-wire for the positive gate voltage V_g between 0 and 0.7 V measured in a similar condition. While the PL of the stem well is unchanged, the PL of the T-wire changes markedly in shape and intensity with changes in the gate bias V_g. For negative bias $V_g < 0$, where electrons are depleted from the T-wire, the PL of the T-wire is quenched. When electrons are accumulated in the T-wire with increasing bias $V_g > 0$, the T-wire PL shows an exciton peak, a charged exciton peak, and a plasma band.

The plasma PL band exhibits lineshapes in which the onset of emission continuously shifts to the red with increasing electron density and the high energy cut-off of the emission is pinned at the position of the charged exciton measured in the limit of very small electron density [25]. The large red-shifts in the PL reveal the band-gap renormalization effect on the optical recombination in the 1D electron plasma.

10. Conclusions

Our recent experiment shows that the origin of gain in a high quality quantum wire laser is not free or localized excitons, but an electron–hole plasma with strong Coulomb correlation. It is also suggested that simple arguments as regards lasing performances in quantum wires based only on the 1D density of states are surely insufficient—more advanced theoretical treatment including Coulomb interactions is necessary.

A stark contrast emerges between undoped and doped T-wires, where experiments show a large band-gap renormalization for one-component electron plasmas and no PL peak shift for neutral two-component electron–hole plasmas. All the results suggest that Coulomb interaction effects are strong in quantum wires and that the intriguing differences between electron and electron–hole plasmas result from a cancellation of the Coulomb interactions in an electron–hole plasma with charge neutrality.

Acknowledgments

We thank Professors T Ogawa at Osaka University, A Pinczuk at Columbia University, P B Littlewood and M H Szymanska at Cambridge University for valuable discussions. We acknowledge the financial support from the MEXT, Japan.

References

[1] Kapon E, Hwang D M and Bhat R 1989 *Phys. Rev. Lett.* **63** 430
[2] Wegscheider W, Pfeiffer L N, Dignam M M, Pinczuk A, West K W, McCall S L and Hull R 1993 *Phys. Rev. Lett.* **71** 4071
Wegscheider W, Pfeiffer L N, West K W and Leibenguth R E 1994 *Appl. Phys. Lett.* **65** 2510
[3] Rossi F and Molinari E 1996 *Phys. Rev. Lett.* **76** 3642
Rossi F and Molinari E 1996 *Phys. Rev.* B **53** 16462
[4] Tassone F and Piermarocchi C 1999 *Phys. Rev. Lett.* **82** 843
Tassone F and Piermarocchi C 2001 *Phys. Rev.* B **63** 5308
[5] Das Sarma S and Wang D W 2000 *Phys. Rev. Lett.* **84** 2010
Das Sarma S and Wang D W 2001 *Phys. Rev.* B **64** 5313

[6] Akiyama H 1998 *J. Phys.: Condens. Matter* **10** 3095
Someya T, Akiyama H and Sakaki H 1996 *Phys. Rev. Lett.* **76** 2965
Someya T, Akiyama H and Sakaki H 1995 *Phys. Rev. Lett.* **74** 3664
Akiyama H, Someya T and Sakaki H 1996 *Phys. Rev.* B **53** R16160
[7] Rubio J, Pfeiffer H, Szymanska M H, Pinczuk A, He S, Baranger H U, Littlewood P B, West K W and Dennis B S 2001 *Solid State Commun.* **120** 423
[8] Ambigapathy R, Bar-Joseph I, Oberli D Y, Haacke S, Brasil M J, Reinhardt F, Kapon E and Deveaud B 1997 *Phys. Rev. Lett.* **78** 3579
[9] Sirigu L, Oberli D Y, Degiorgi L, Rudra A and Kapon E 2000 *Phys. Rev.* B **61** R10575
[10] Arakawa Y and Sakaki H 1982 *Appl. Phys. Lett.* **40** 939
[11] Asada M, Miyamoto Y and Suematsu Y 1985 *Japan. J. Appl. Phys.* **24** L95
[12] Szymanska M H, Littlewood P B and Needs R J 2001 *Phys. Rev.* B **63** 205317
[13] Pfeiffer L N, West K W, Stormer H L, Eisenstein J P, Baldwin K W, Gershoni D and Spector J 1990 *Appl. Phys. Lett.* **56** 1697
[14] Yoshita M, Akiyama H, Pfeiffer L N and West K W 2001 *Japan. J. Appl. Phys.* 2 **40** L252
[15] Yoshita M, Akiyama H, Pfeiffer L N and West K W 2002 *Appl. Phys. Lett.* **81** 49
Yoshita M, Oh J W, Akiyama H, Pfeiffer L N and West K W 2003 *J. Cryst. Growth* **251** 62
[16] Oh J W, Yoshita M, Akiyama H, Pfeiffer L N and West K W 2003 *Appl. Phys. Lett.* **82** 1709
[17] Ishii A, Aisaka T, Oh J W, Yoshita M and Akiyama H 2003 *Appl. Phys. Lett.* **83** 4187
[18] Akiyama H, Yoshita M, Pfeiffer L N, West K W and Pinczuk A 2003 *Appl. Phys. Lett.* **82** 379
[19] Ogawa T and Takagahara T 1991 *Phys. Rev.* B **43** 14325
Ogawa T and Takagahara T 1991 *Phys. Rev.* B **44** 8138
[20] Itoh H, Hayamizu Y, Yoshita M, Akiyama H, Pfeiffer L N, West K W, Szymanska M H and Littlewood P B 2003 *Appl. Phys. Lett.* **83** 2043
[21] Akiyama H, Pfeiffer L N, Yoshita M, Pinczuk A, Littlewood P B, West K W, Matthews M J and Wynn J 2003 *Phys. Rev.* B **67** 041302(R)
[22] Takahashi Y, Watanabe S, Yoshita M, Itoh H, Hayamizu Y, Akiyama H, Pfeiffer L N and West K W 2003 *Appl. Phys. Lett.* **83** 4089
[23] Hayamizu Y, Yoshita M, Watanabe S, Akiyama H, Pfeiffer L N and West K W 2002 *Appl. Phys. Lett.* **81** 4937
[24] Akiyama H, Pfeiffer L N, Pinczuk A, West K W and Yoshita M 2002 *Solid State Commun.* **122** 169
[25] Takagiwa M and Ogawa T 2002 *J. Phys. Chem. Solids* **63** 1587